LBL-25971 c.2

Lawrence Berkeley Laboratory
UNIVERSITY OF CALIFORNIA

EARTH SCIENCES DIVISION

Some Design Considerations for the Proposed Dixie Valley Tracer Test

C. Doughty and G.S. Bodvarsson

June 1988

Prepared for the U.S. Department of Energy under Contract Number DE-AC03-76SF00098.

DISCLAIMER

LBL-25971

Some Design Considerations for the Proposed Dixie Valley Tracer Test

Christine Doughty
Gudmundur S. Bodvarsson

Earth Sciences Division
Lawrence Berkeley Laboratory
1 Cyclotron Road
Berkeley, California 94720

June 1988

This work was supported by the Assistant Secretary for Conservation and Renewable Energy, Office of Renewable Energy Technologies, Geothermal Technology Division, of the U.S. Department of Energy under Contract No. DE-AC03-76SF00098.

Introduction

A tracer test for the Dixie Valley, Nevada, geothermal resource is planned for the summer of 1988, in order to study the fluid flow paths that will develop under typical operating conditions. During the test six production wells will provide the power plant with steam sufficient for generation of 60 MWe, requiring fluid production at a rate of approximately 600 kg/sec. Up to 75% by mass of the extracted fluid will be reinjected into the reservoir, using four injection wells. Tracer will be added to the injected fluid for a twenty-minute period, and subsequently the produced fluid will be monitored for the tracer.

To help in determining the quantity of tracer to inject, and where and when to look for breakthrough, we have mathematically modeled the proposed tracer test using a three-dimensional porous medium model developed in 1986 and 1987 by the Oxbow Geothermal Corporation (Oxbow, 1986, 1987). The mathematical model assumes fluid flow at the Dixie Valley geothermal field is primarily through high-permeability channels associated with the SW-NE trending range-front fault that separates Dixie Valley from the adjacent Stillwater Range. A plan view of the model is shown in Figure 1. Each zone labeled 1-7 is further discretized, as shown in Figure 2, which is a cross-section through zone 1. Figure 3 shows a conceptual model of the reservoir in a cross-section perpendicular to that of Figure 2, with well locations projected onto the plane of the range-front fault. The model was developed from an integrated analysis of geological, geochemical, and seismological data, natural-state modeling of the system, and modeling of two extensive flow tests. The rather coarse spatial discretization, which is deemed appropriate for natural-state, flow-test, and production modeling, is less accurate for tracer-test modeling, so the following results should be viewed as general estimates of future behavior, rather than detailed predictions.

The lateral heat and fluid flow boundary conditions are shown in Figure 1. The vertical boundaries are closed to fluid flow, except for a localized recharge region modeled with a mass source in element 1199 (at the range-front fault in zone 1, see Figure 2). The recharge rate was determined through natural-state modeling. Heat flow above and below the modeled region is assumed to be conductive. Initial conditions for the tracer test simulation are taken to be the final conditions of a one-year predictive calculation made in 1987 following a flow-test history match.

The computer program MULKOM (Pruess, 1983), developed at Lawrence Berkeley Laboratory (LBL), is used for the calculations. MULKOM uses the Integral-Finite-Difference method to calculate coupled flows of water and carbon dioxide (in liquid and vapor phases), and heat in fractured/porous media. For the modeling of the proposed Dixie Valley tracer tests we introduce carbon dioxide as a conservative tracer dissolved in the liquid phase. Under natural state and expected exploitation conditions at Dixie Valley, water will remain single-phase liquid, so that CO_2 in liquid is an acceptable and simple way to simulate a tracer.

Production during the tracer test will be from wells 27-33, 45-33, 76-7, 74-7, 73-7, and 84-7 (see Figure 1). These wells will produce at a near-constant line pressure, with the flow rate declining as determined from measured flow rate/pressure decline curves. The wells will be put on line as needed to maintain 60 MWe. The total mass flow rate is estimated to be 592 kg/sec; initial production flow rates are shown in Table 1 for each well. Injection will be into wells 45-5, 32-18, 52-18, and 65-18 at the estimated rates shown in Table 1.

Table 1. Initial production rates and estimated injection rates.

Well	Production Rate (kg/s)	Well	Injection Rate (gpm)	(kg/s)*
27-33	85	52-18	1000	60.4
45-33	108	65-18	1300	78.6
76-7	174	32-18	1700	102.8
73-7	55	45-5	2000	120.9
74-7	170			
84-7	0			
Total	592	Total	6000	362.7

*Assumes the density of injected water is 958 kg/m^3

Cases Considered

A summary of the cases considered is shown in Table 2. The cases labeled with a P use the porous medium model described above. The cases labeled with an F use a simple fractured medium model, derived from the porous medium model as follows. Assuming a fracture porosity of 1%, the volume of all elements is decreased by a factor of 100, total compressibility (rock plus water) is increased by a factor of 100, and rock heat capacity is increased by a factor of 100. This allows an approximate calculation of fracture flow, maintaining the appropriate pressure decline and thermal front movement. However, it is important to note that the assumption of 1% fracture porosity is only a first-order estimate, which greatly affects the results obtained. Hence, all results should only be considered as first-order estimates. A brief discussion of each case follows.

Table 2. Cases Considered

Case	Power (MWe)	Duration (Years)	Injection Percentage	Tracer Injection Well	Tracer Injection Duration
P10	51	5	75	All	10 Days
P21	60	5	61	All	20 Minutes
F22	60	1/2	61	All	20 Minutes
F23	60	1	61	65-18	20 Minutes
F24	60	1	61	45-5	20 Minutes
F25	60	1	61	32-18	20 Minutes
F26	60	1	61	52-18	20 Minutes

P10 The first case considered uses the porous medium model, with somewhat different injection and production conditions. A five-year simulation is carried out in which a 51 MWe power production rate is prescribed. MULKOM calculates that extraction of 503 kg/sec of fluid is required to supply this power generation. Injection is specified at 1050 gpm (63 kg/sec) into wells 65-18 and 52-18 and at 2100 gpm (127 kg/sec) into wells 32-18 and 45-5, for a total of 380 kg/sec, about 75% of the fluid produced. After one month of production a 10-day slug of tracer is injected at a constant concentration C_0. Figures 4a, 4b, and 4c show the tracer concentrations in the elements containing the injection and production wells as a function of time. Note the different vertical scales for the different figures. The large volumes of the elements containing the wells results in a large dilution of concentration. The mesh coarseness also distorts the time variation of the tracer pulse. In the injection wells, the tracer concentration builds up rapidly but declines much more slowly (Figure 4a). There are still appreciable levels of tracer after two years in 32-18 and 45-5, and after four years in 52-18 and 65-18. This variation should be viewed as representing the region around the injection well, rather than the well itself, in light of the coarse mesh used. The lower concentration levels and slower decline from wells 52-18 and 65-18 result from the larger volumes of the elements in which these wells are located. With the above considerations in mind, the most valid interpretation of the modeled tracer concentrations is to not believe absolute values of either the breakthrough times or concentration levels, but to consider the responses of the different production wells relative to one another. In production well 76-7, tracer breakthrough occurs about two months after tracer injection, with a maximum concentration occuring after about three years (Figure 4b). Tracer breakthrough in wells 84-7 and 74-7 occurs about four to six months after tracer injection, but at very low concentrations; the breakthrough in well 73-7 occurs after about 1.5 years (Figure 4c). In wells 84-7, 74-7, and 73-7 tracer concentration is still increasing after five years. Although these times are fictitious due to the coarse mesh used, the earlier response to the tracer pulse indicates well 76-7 is better connected to the injection wells. Our calculations show no noticeable tracer in wells 27-33 and 45-33, indicating low connectivity.

P21 After the above preliminary calculation was made, further details of the tracer test were incorporated in the model: the duration of the tracer injection was decreased from 10 days to 20 minutes, power generation was increased from 51 to 60 MWe, and the flow rates from Table 1 were employed. With the increase in power generation, a total fluid production rate of 592 kg/sec is required, so the injection of 363 kg/sec (Table 1) results in 61% reinjection. With the shorter tracer injection period, far less tracer is injected and the porous medium model shows such a small tracer response in the producing wells that the use of the more realistic fractured medium model is necessary.

F22 The fractured medium model is used to calculate a six-month 60 MWe production period with 6000 gpm injection, as specified in Table 1. A twenty-minute tracer slug is added to all injection wells after 31 days of production. Figure 5a shows the tracer concentrations in the injection wells. Figure 5b shows the tracer concentrations in the production wells. All production wells show some tracer within six months, although for well 73-7 the level is very low. Figure 5c shows early-time behavior at the production wells. Tracer breakthrough times of 1, 4, and 6 days after tracer injection are estimated for wells 76-7, 84-7, and 74-7, respectively. Tracer breakthroughs in wells 45-33 and 27-33 occur after a much longer time, about 30 days after tracer injection. Tracer breakthrough in well 73-7 is estimated to be the slowest and tracer concentration the lowest.

F23 To better study the connectivity between the various injection and production wells, simulations were done in which tracer is injected into only one injection well at a time. These simulations are carried out for a one year period. In each case the injection and production rates from Table 1 are used. In this case tracer is only injected into well 65-18. Figures 6a and 6b show tracer concentration in the production wells. Wells 76-7, 74-7, and 84-7 show similar responses, well 73-7 shows a much smaller response, and wells 27-33 and 45-33 show no response at all.

F24 In this case tracer is only injected into well 45-5. Figure 7 shows tracer concentration in the production wells. Wells 27-33 and 45-33 show the largest response, well 73-7, 74-7, and 84-7 show a smaller response, and well 76-7 shows no response.

F25 In this case tracer is only injected into well 32-18. Figures 8a and 8b show tracer concentration in the production wells. Well 76-7 shows the greatest response, followed by well 84-7, 74-7, and 73-7, in decreasing order. Wells 27-33 and 45-33 show no response.

F26 In this case tracer is only injected into well 52-18. Figures 9a and 9b show tracer concentration in the production wells. Overall the response is similar to that for case F23, but with a slight time shift.

Comparison with UURI Radial Model

Table 3 shows a summary of the results obtained by the University of Utah Research Institute (UURI), using a quasi-radial flow model (M. Adams and J. Moore, personal communication, 1988). The UURI work predicts the required mass of tracer, M_{inj}, to inject in order to obtain a peak tracer concentration of 60 ppb at the nearest production well. The tracer detection limit is considered to be 60 ppb, although in reality the actual detection limit of most of the tracers planned for Dixie Valley is about three times lower. Hence, the results and analyses include a safety factor of three.

Table 3. Summary of UURI radial model results.

Injection Well	D (m)	h (m)	M_w (kg)	M_{inj} (kg)
65-18	1730	22	3.5×10^9	213
45-5	2000	153	3.3×10^{10}	1982
32-18	1400	19	2.0×10^9	119
52-18	1100	109	7.1×10^9	425

According to the quasi-radial flow model used in the UURI work, the mass of water in the zone swept by tracer at breakthrough, M_w, is given by

$$M_w = 1.076D^2h\,\phi\rho_w$$

where D is the average distance between the injection well and the production wells, h is the average open interval of the injection well and the production wells, porosity ϕ=0.05, and water density ρ_w=1000 kg/m^3. The quantity M_w is called the maximum dilution. The required mass of tracer to inject, M_{inj}, is then

$$M_{inj} = C_{dl}M_w$$

where C_{dl}=60 ppb $=6\times10^{-8}$ is the tracer detection limit.

In order to compare our calculations to the UURI work, in Table 4 we present the results of cases F23, F24, F25, and F26 in terms of M_w and M_{inj}.

Table 4. Summary of LBL 3-D model results.

Injection Well	M_{inj}^N (kg)	Production Well	C_{pk}^N	t_{bt}^N (days)	t_{pk}^N (days)	M_w (kg)	M_{inj} (kg)
65-18	94,300	76-7	1.48×10^{-5}	11	102	6.37×10^{9}	382
		84-7	1.23×10^{-5}	15	148	7.67×10^{9}	460
		74-7	1.29×10^{-5}	12	125	7.31×10^{9}	439
		73-7	2.21×10^{-7}	34	171	4.27×10^{11}	25,600
		27-33	–	–	–		
		45-33	–	–	–		
45-5	145,000	76-7	–	–	–		
		84-7	5.78×10^{-6}	49	216	2.51×10^{10}	1506
		74-7	6.78×10^{-6}	49	193	2.14×10^{10}	1284
		73-7	1.04×10^{-5}	49	273	1.39×10^{10}	837
		27-33	3.22×10^{-5}	19	171	4.51×10^{9}	270
		45-33	3.29×10^{-5}	19	159	4.41×10^{9}	265
32-18	123,500	76-7	2.29×10^{-4}	1	11	5.39×10^{8}	32
		84-7	1.23×10^{-5}	4	45	1.00×10^{10}	602
		74-7	1.73×10^{-6}	9	114	7.14×10^{10}	4283
		73-7	5.99×10^{-7}	5	57	2.06×10^{11}	12,370
		27-33	–	–	–		
		45-33	–	–	–		
52-18	72,500	76-7	2.68×10^{-5}	3	51	2.70×10^{9}	162
		84-7	1.74×10^{-5}	6	91	4.17×10^{9}	250
		74-7	2.09×10^{-5}	4	68	3.47×10^{9}	208
		73-7	2.09×10^{-7}	9	91	3.47×10^{11}	20,810
		27-33	–	–	–		
		45-33	–	–	–		

The mass of CO_2 injected in the numerical model is M_{inj}^N. The peak CO_2 concentration at a production well is C_{pk}^N; it occurs at time t_{pk}^N. The time at which CO_2 is first observed at a production well is t_{bt}^N. Times are measured relative to the start of tracer injection. The quantities M_{inj}^N and C_{pk}^N can be used to determine maximum dilution as

$$M_w = \frac{M_{inj}^N}{C_{pk}^N}$$

Thus, the required mass to inject in order to obtain a peak tracer concentration of C_{dl} =60 ppb (=6×10^{-8}) is

$$M_{inj} = C_{dl}\, M_w = C_{dl}\, \frac{M_{inj}^N}{C_{pk}^N}$$

Discussion

The wide range of values of M_{inj} for each injection well, listed in Table 4, shows that the amount of tracer required for 60 ppb detection depends strongly on which production well is being monitored. For example, the results obtained suggest that for tracer injected into well 45-5 to be detected at wells 84-7, 74-7, and 73-7 about 1500 kg of tracer should be injected. However, the same tracer may be detected in wells 27-33 and 45-33 with only 300 kg of tracer injected. Thus, one must weigh the cost of the tracer versus the number of wells that will detect it, to arrive at the best estimate for the amount of tracer that should be injected.

When comparing the results of the radial and 3-D models it should be noted that the two models assume vastly different flow fields, so close agreement in predicted values of M_w and M_{inj} is not expected. Based on previous modeling studies (Oxbow, 1986, 1987) a radial flow field is not expected at Dixie Valley due to the dominant influence of the range-front fault, indicating that the 3-D model results are probably more reliable. However, the coarse mesh and simplistic fractured medium representation limit accuracy of the 3-D model as well.

If we for a moment pretend to believe the results given by the numerical model, the following points may be considered.

Well 32-18 has by far the best hydraulic communication with well 76-7, although the model suggests that if sufficient tracer were injected in well 32-18, tracer would also reach wells 84-7 and 74-7. However, we can argue that since the vast majority of the fluids injected into well 32-18 will arrive at well 76-7, it would be a waste of money to inject sufficient tracer to attempt to get a breakthrough in wells 84-7 and 74-7. Furthermore, if we only attempt to get breakthrough at one well, we want to make sure that it actually will occur and inject a conservative amount of tracer. Hence, if we believed the 3-D model results, we would inject some 100 kg of tracer into well 32-18 and look for it in well 76-7.

A similar line of reasoning can be applied to the other injection wells, but we may not want to be as conservative as in the case of well 32-18 because of the larger masses of tracer, and hence costs, involved. In the case of well 45-5 we suggest looking for breakthrough in wells 27-33 and 45-33. The 3-D model indicates that the amount of tracer needed to get detectable breakthrough in these wells is about 300 kg. We would be conservative with the relatively cheap tracer (BSA) and inject 600-900 kg in order to make breakthrough in wells 45-33 and 27-33 likely. Due to its higher cost, we would inject only about 150 kg of dye, a marginal amount to get breakthrough of 30 ppb, the dye detection limit.

The 3-D model results suggest that the amount of tracer required in wells 52-18 and 65-18 to get detectable breakthrough in wells 76-7, 84-7, and 74-7 is approximately 300 and 500 kg, respectively. It may be beneficial to use conservative amounts of tracer for well 52-18, which we believe has a much higher chance of yielding tracer breakthroughs in the section 7 wells, and only marginal quantities in well 65-18, to minimize costs.

Now back to reality, as one must recognize the uncertainties involved in these calculations. The relationship between fracture porosity and both tracer breakthrough time and peak concentration is approximately linear. That is, a fracture porosity of 5% instead of 1% would yield tracer breakthrough times about five times longer and peak concentrations about five times smaller than those shown in the present report. Thus the estimates given are very uncertain and should only be used as relative guidelines.

Even if fracture porosity were known accurately, the present results would have to be used with caution because numerical codes tend to smear out chemical fronts due to numerical dispersion, causing the calculated peak concentrations to be many times too low. This smearing is rather obvious when one inspects the computed tracer curves, which show very diffuse maxima.

Another factor that should be considered in the design of the tracer test is experience obtained from tracer tests in other parts of the world. One of the best papers available is that by Urbino et al (1986), on tracer tests conducted at the Palinpinon geothermal field in the Philippines. They injected a total of 10 kg of dye into an injector and saw tracer breakthroughs in about ten production wells located 800-1500 m away in one to ten days. Although the Palinpinon reservoir has vastly different structural control than the Dixie Valley system, this suggests that perhaps all of our calculations are very conservative.

Table 5 shows tracer migration velocities determined from tracer tests or enthalpy transients for several geothermal fields with major vertical fractures (Pruess and Bodvarsson, 1984). It is clear that velocity varies widely not only between fields, but also among wells in the same field. The tracer breakthrough time given in Table 5 and the distance between wells from Table 3 may be combined to approximate tracer migration velocity for Dixie Valley as $v = D / t_{bt}^N$. (The value of t_{bt}^N for well 74-7 is used because the distances from well 74-7 to the injection wells best match the D values from Table 3.) The calculated tracer migration velocities fall within the range of the field values.

Table 5. Observed tracer migration velocities for several geothermal fields with major vertical fractures and calculated values for Dixie Valley.

Observed Velocities		
Geothermal Field	Distance Between Wells, D (m)	Tracer Migration Velocity, v (m/hr)
Wairakei	500	2.7
	145	0.7
	230	1.1
	500	8.0
Ohaaki	270	0.4
	75	0.4
Hatchobaru	140	6.1
	135	33.8
	180	9.0
Otake	125	0.2
	203	0.3
	140	0.2
Tongonan	400	57.0
	200	30.0
	200	22.0
Calculated Velocities for Dixie Valley		
Well	D (m)	v (m/hr)
65-18	1730	6
45-5	2000	2
32-18	1400	6
52-18	1100	11

Acknowledgements

The authors would like to thank Oxbow Geothermal Corporation for allowing use of their model for this work, and I. Javandel, M.J. Lippmann, and K. Pruess for their careful review of this paper. This work was supported by the Assistant Secretary for Conservation and Renewable Energy, Office of Renewable Energy Technologies, Geothermal Technology Division, of the U.S. Department of Energy under Contract No. DE-AC03-76SF00098.

References

1. Oxbow Geothermal Corporation, Dixie Valley Reservoir Assessment, October 28, 1986.
2. Oxbow Geothermal Corporation, Six-well Flow Test, Dixie Valley, Nevada July 23, 1986 – July 1, 1987, October 26, 1987.
3. Pruess, K., Development of the General Purpose Simulator MULKOM, Annual Report 1982, Earth Sciences Division, *Rep. LBL-15500*, Lawrence Berkeley Laboratory, 1983.
4. Urbino, M. E. G., Zaide, M. C., Malate, R. C. M., and Bueza, E. L., Structural flowpaths of reinjected fluids based on tracer tests – Palinpinon I, Philippines, Proceedings of the 8th New Zealand Geothermal Workshop, 1986.
5. Pruess, K. and Bodvarsson, G. S., Thermal effects of reinjection in geothermal reservoirs with major vertical fractures, *J. of Petroleum Tech.*, pp. 1567-1578, September, 1984.

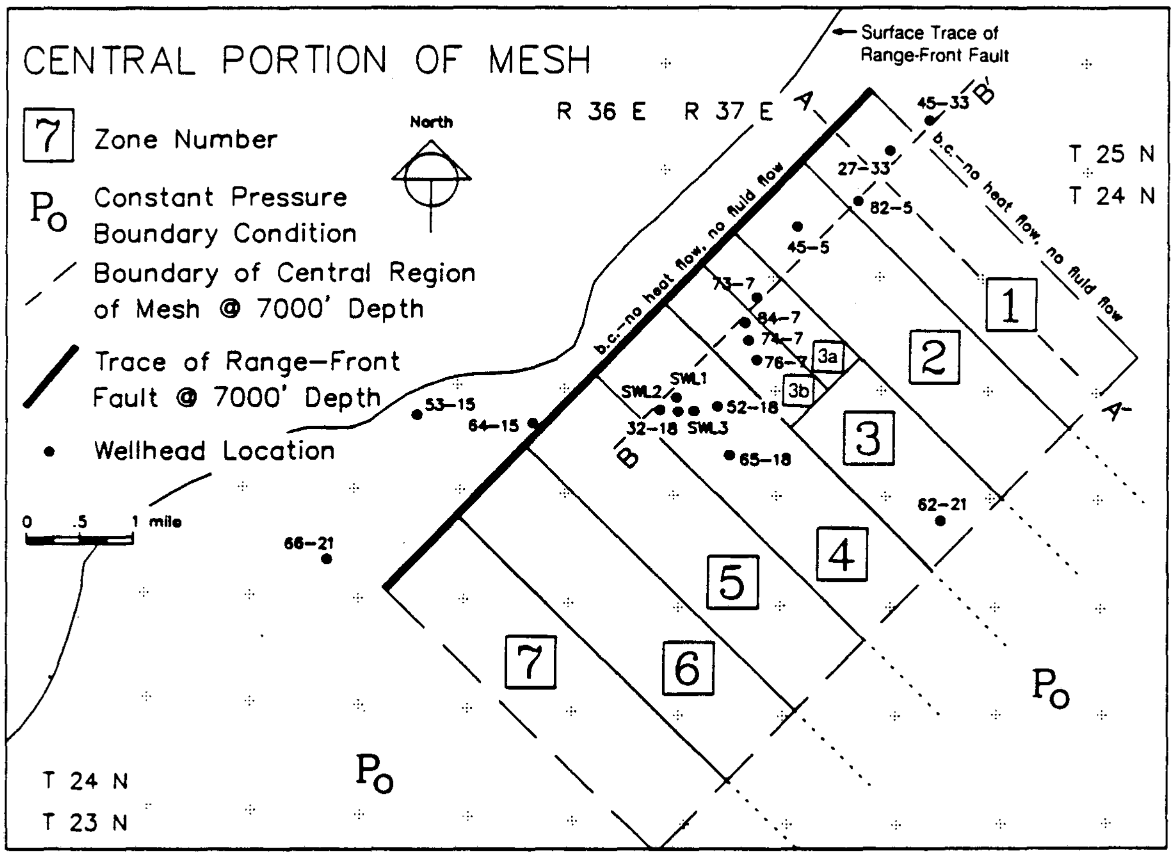

XBL 889-10416

1. Plan view of the central portion of the calculational mesh, showing the well field and range-front fault (after Oxbow, 1986, 1987). Each zone 1-7 is further discretized, as shown in Figure 2 for zone 1.

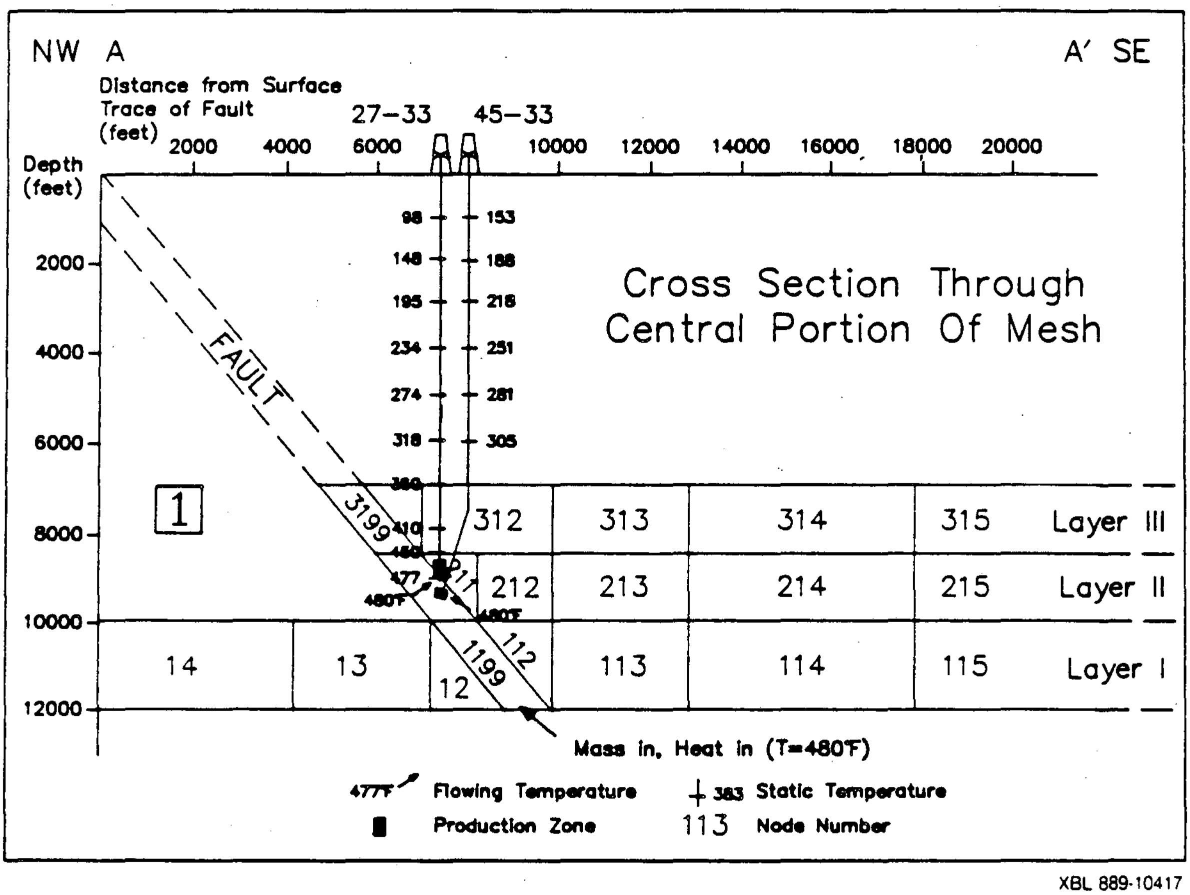

2. Cross-sectional view of zone 1 of the calculational mesh (after Oxbow, 1986, 1987). A-A′ shows cross-section location in Figure 1.

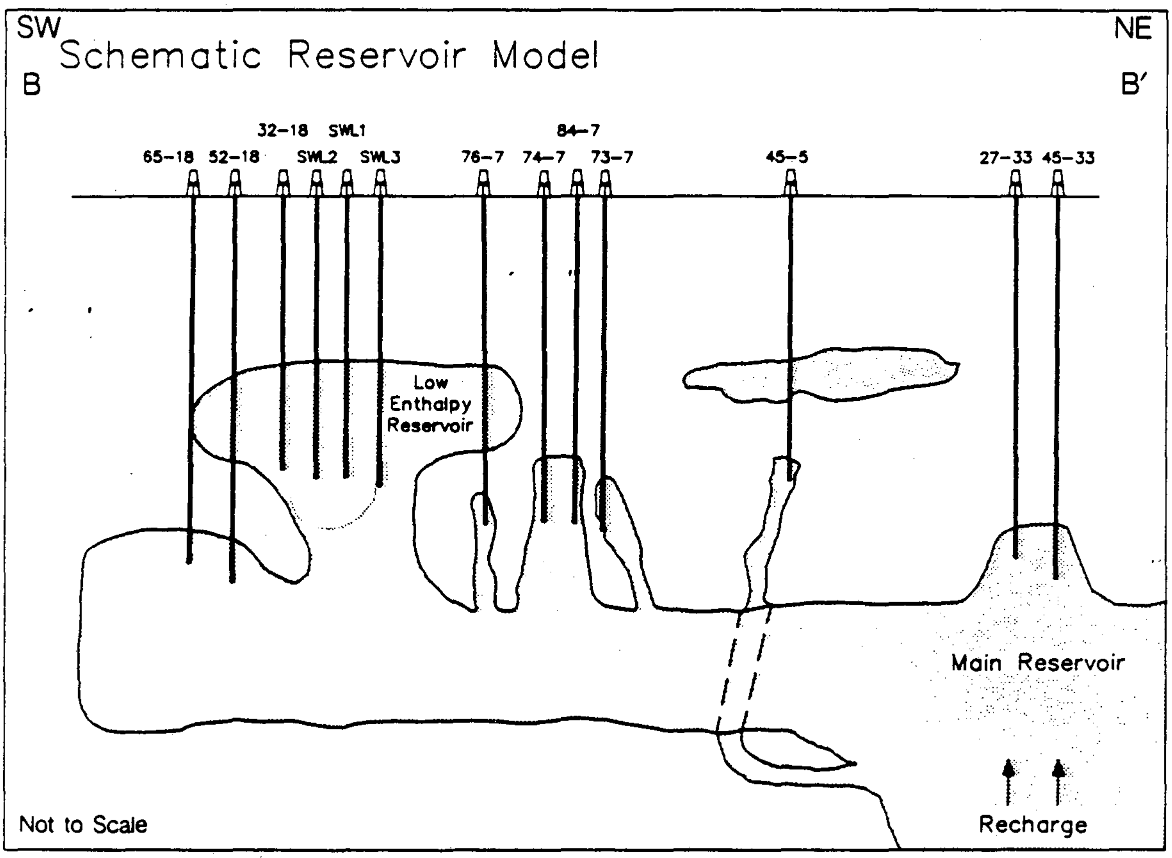

XBL 889-10418

3. Schematic model of the Dixie Valley Reservoir (Oxbow, 1987). B-B′ shows cross-section location in Figure 1.

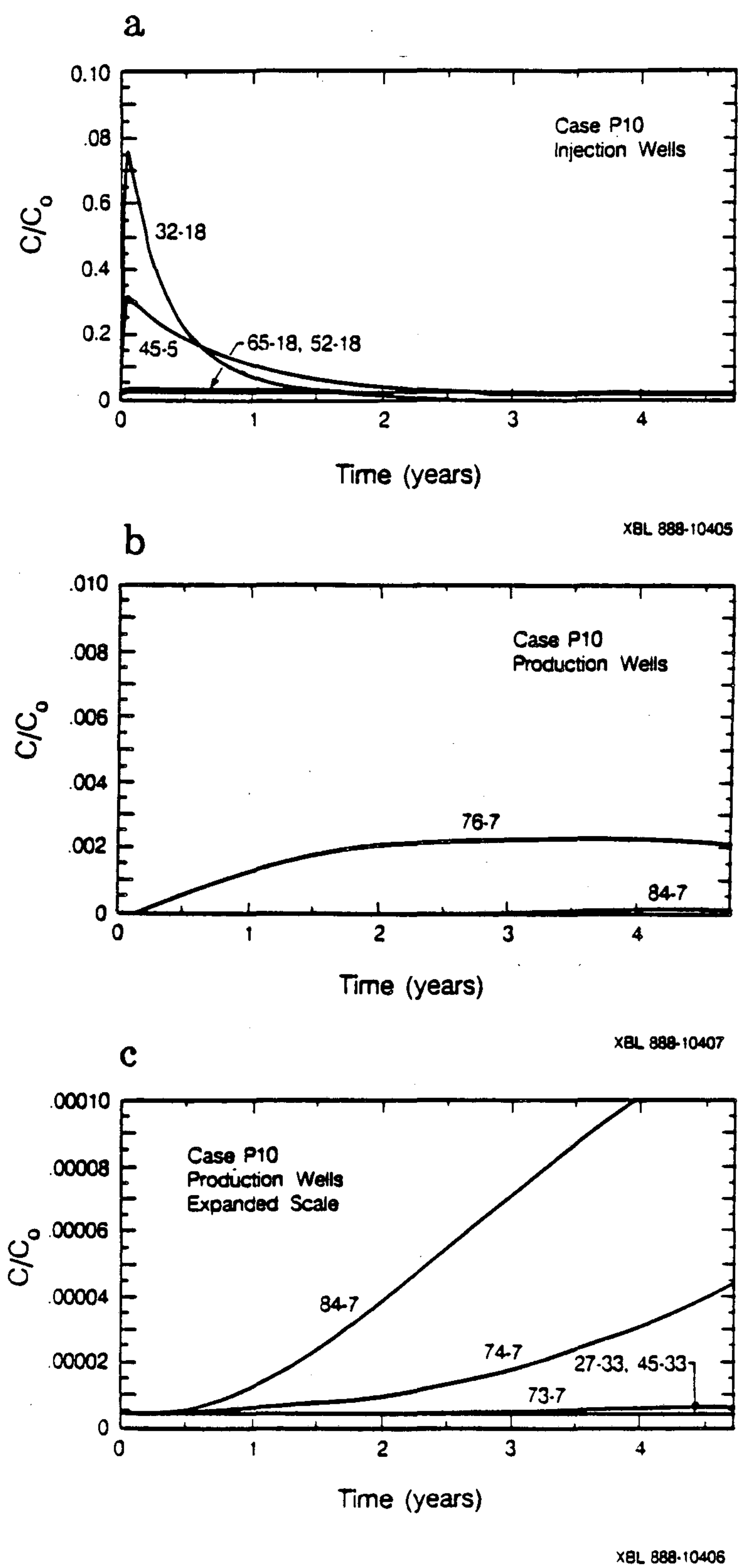

4. Tracer concentration for case P10 for the injection wells and the production wells.

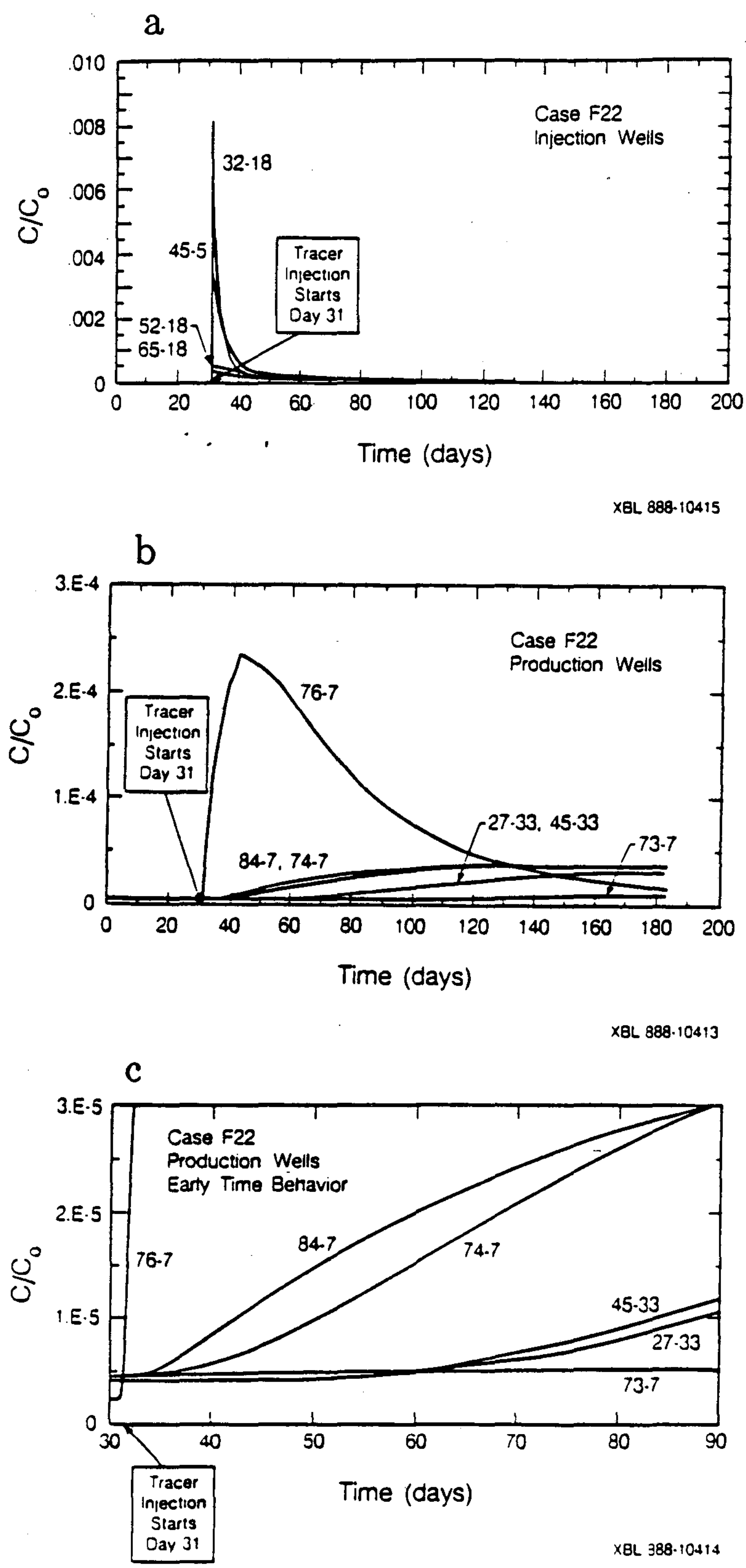

5. Tracer concentration for case F22 for the injection wells and the production wells.

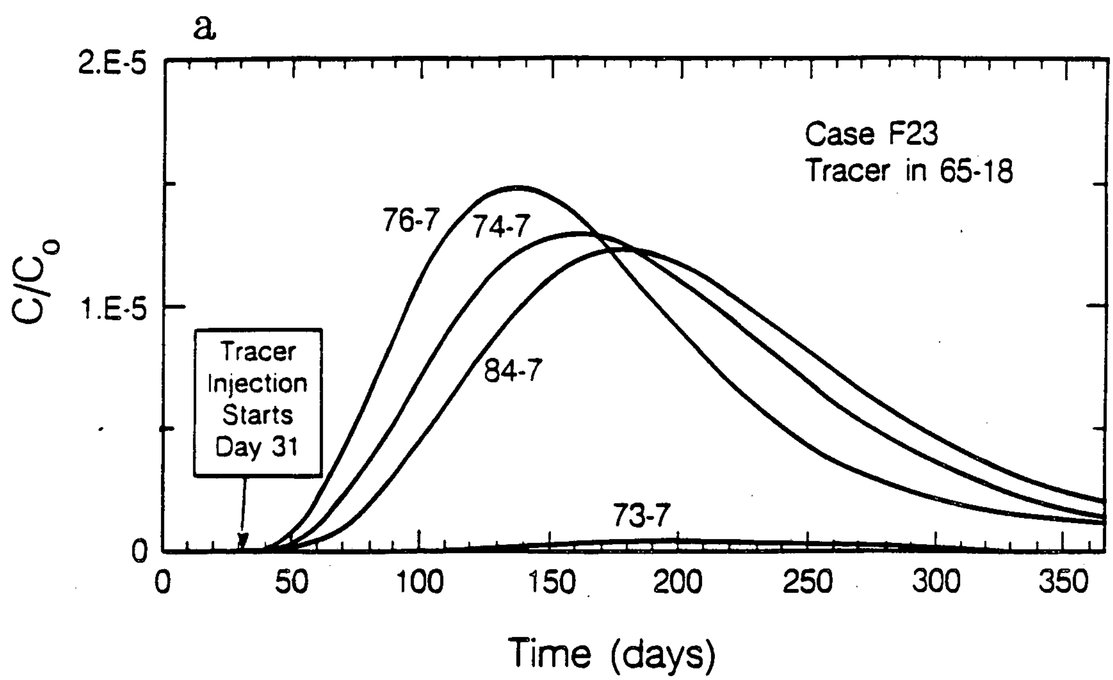

XBL 888-10412

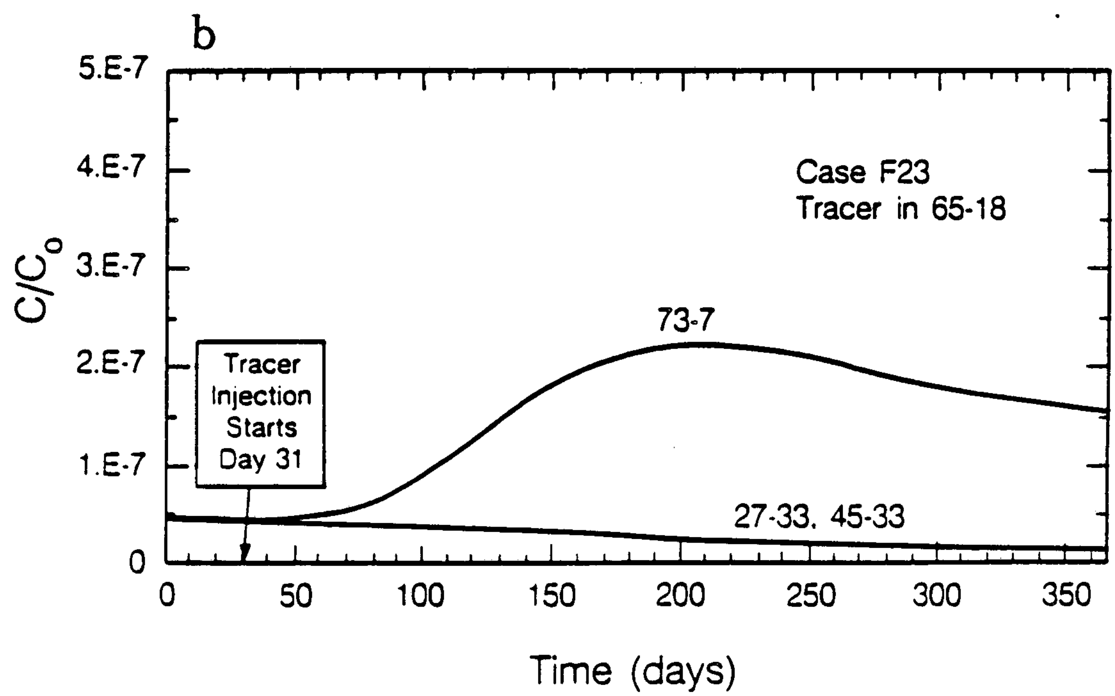

XBL 888-10404

6. Tracer concentration for case F23 for the production wells.

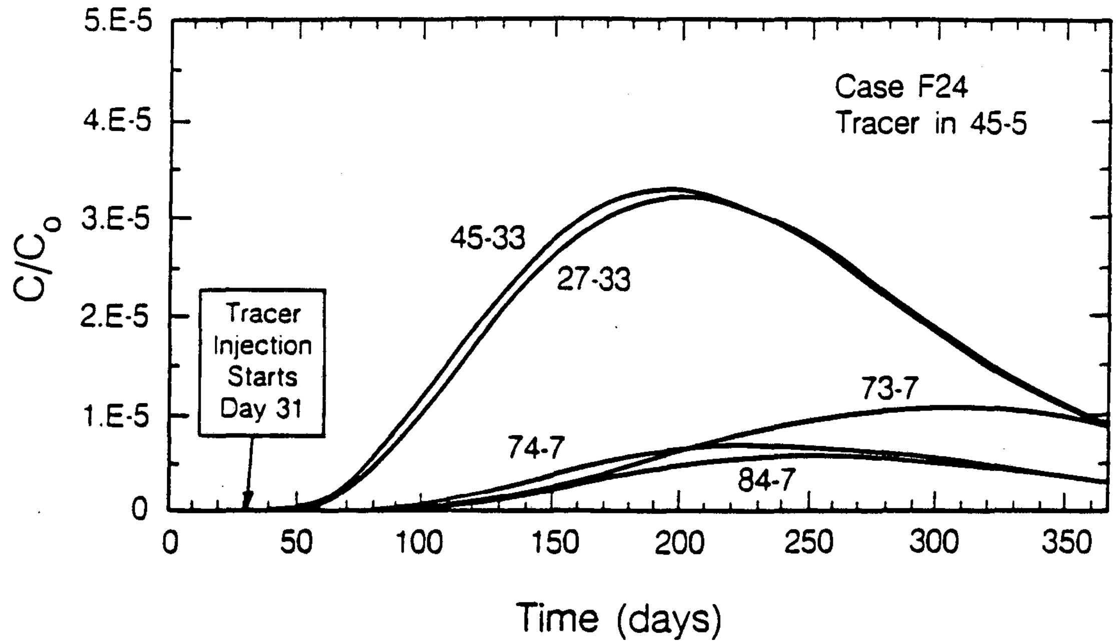

XBL 888-10403

7. Tracer concentration for case F24 for the production wells.

a

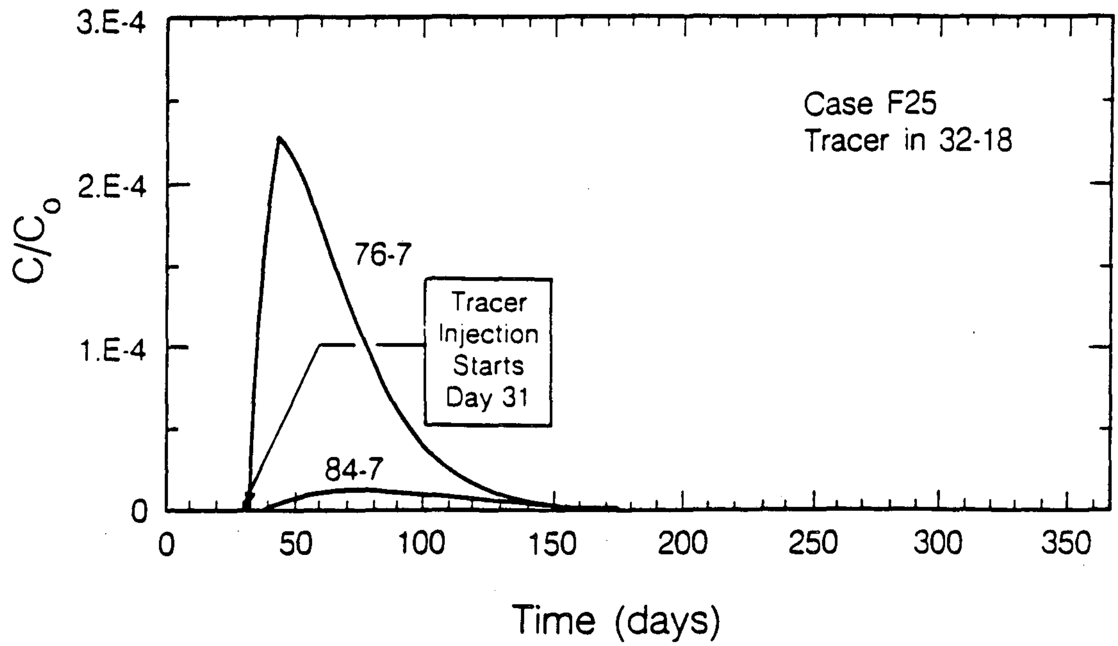

XBL 888-10410

b

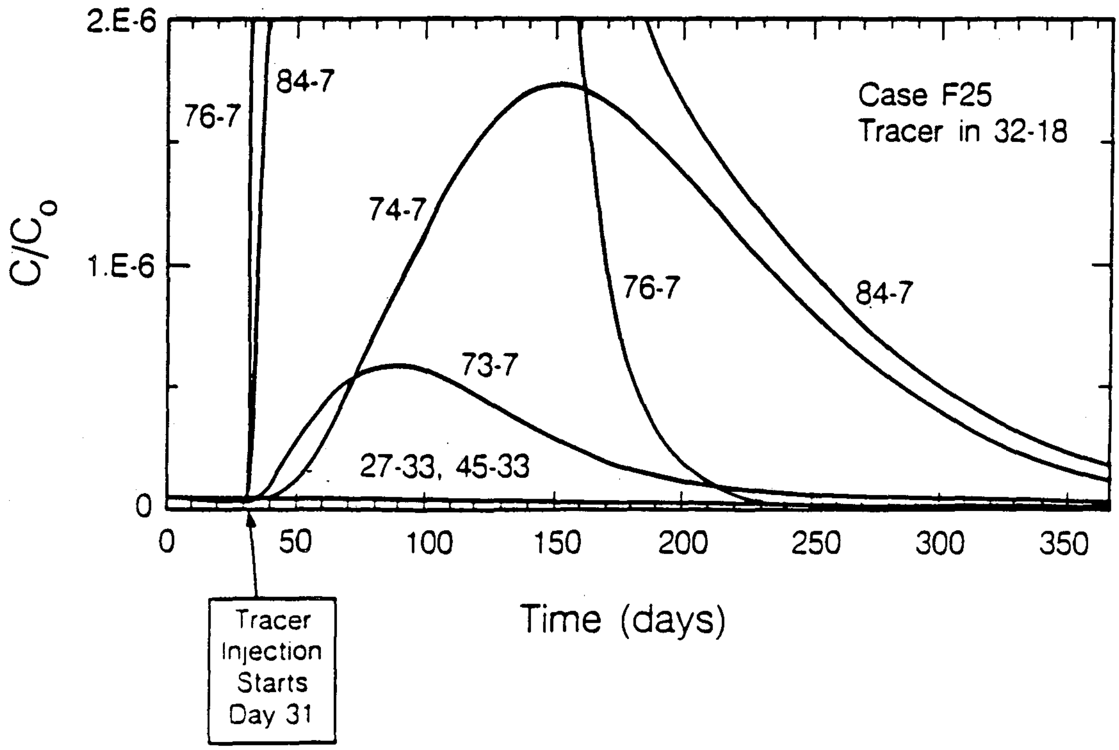

XBL 888-10411

8. Tracer concentration for case F25 for the production wells.

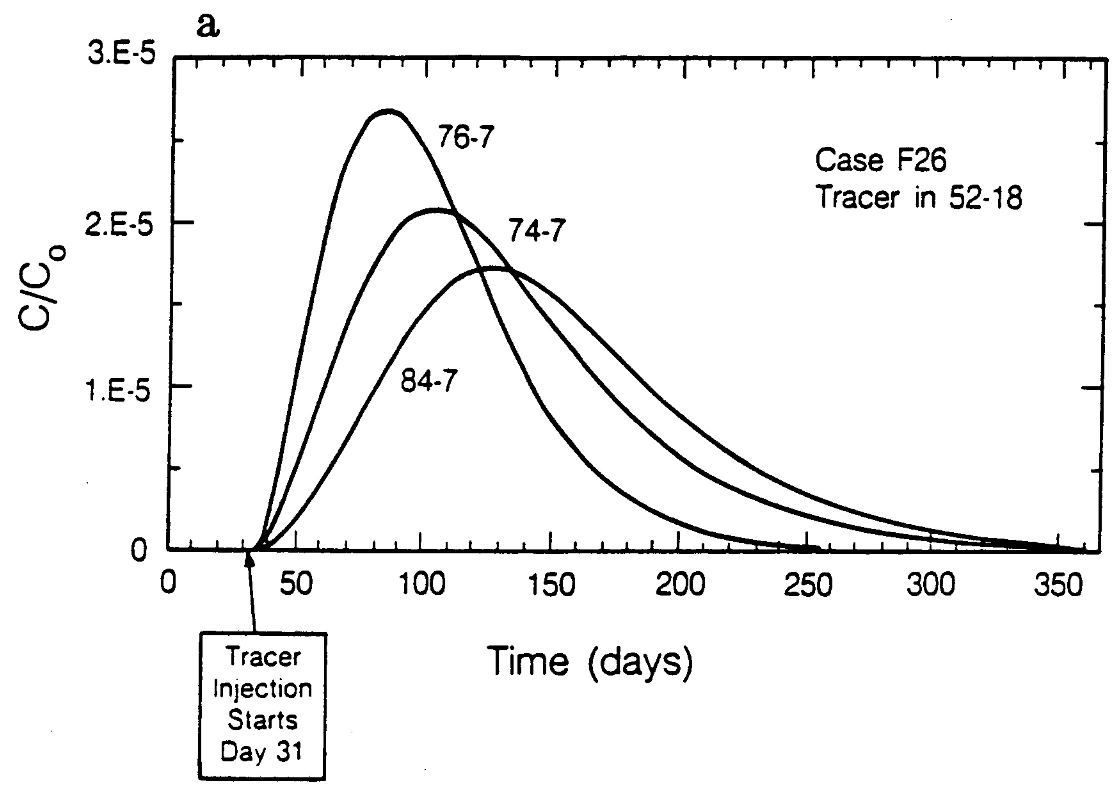

XBL 888-10409

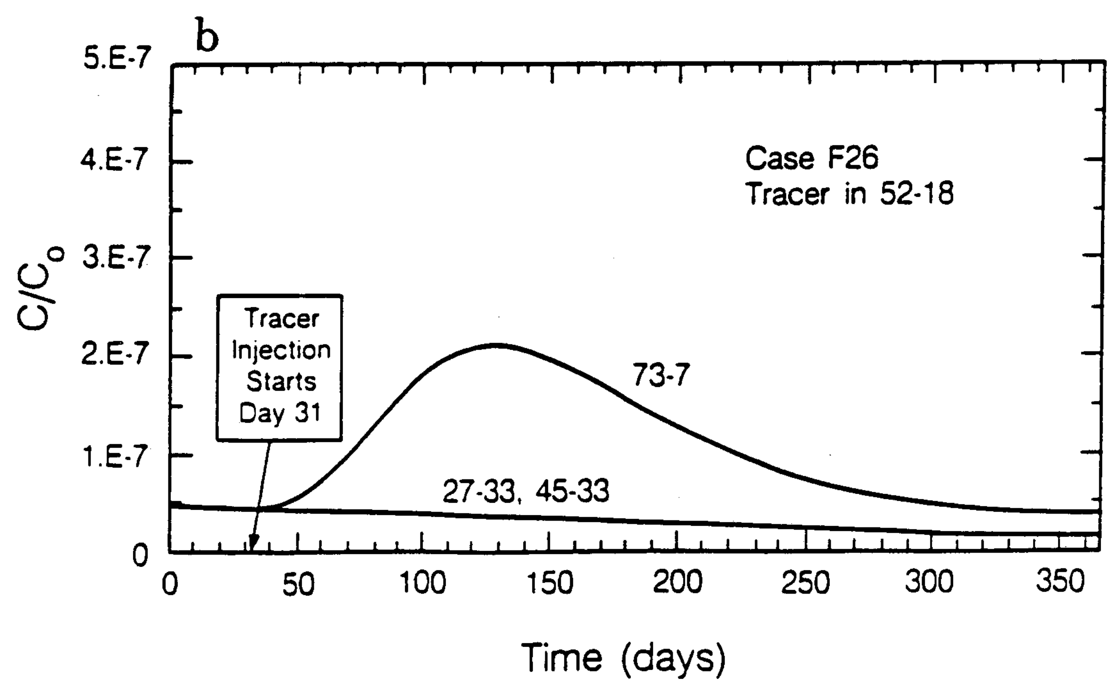

XBL 888-10408

9. Tracer concentration for case F26 for the production wells.